1-1-2016

Toward biodegradable Mg-air bioelectric batteries composed of silk fibroin-polypyrrole film

Xiaoteng Jia
University of Wollongong, xj916@uowmail.edu.au

Caiyun Wang
University of Wollongong, caiyun@uow.edu.au

Chen Zhao
University of Wollongong, cz995@uowmail.edu.au

Yu Ge
University of Wollongong, yg711@uowmail.edu.au

Gordon G. Wallace
University of Wollongong, gwallace@uow.edu.au

Toward biodegradable Mg-air bioelectric batteries composed of silk fibroin-polypyrrole film

Abstract

Biodegradable active implantable devices can be used to diagnose and/or treat disease and eventually disappear without surgical removal. If an "external" energy source is required for effective operation then a biocompatible and biodegradable battery would be ideal. In this study, a partially biodegradable Mg-air bioelectric battery (biobattery) is demonstrated using a silk fibroin-polypyrrole (SF-PPy) film cathode coupled with bioresorbable Mg alloy anode in phosphate buffered saline (PBS) electrolyte. PPy is chemically coated onto one side of the silk substrate. SF-PPy film shows a conductivity of ≈1.1 S cm−1 and a mild catalytic activity toward oxygen reduction. It degrades in a concentrated buffered protease XIV solution, with a weight loss of 82% after 15 d. The assembled Mg-air biobattery exhibits a discharge capacity up to 3.79 mA h cm−2 at a current of 10 μA cm−2 at room temperature, offering a specific energy density of ≈4.70 mW h cm−2. This novel partially biodegradable battery provides another step along the route to biodegradable batteries.

Keywords

toward, fibroin, polypyrrole, film, batteries, composed, bioelectric, air, silk, mg, biodegradable

Disciplines

Engineering | Physical Sciences and Mathematics

Publication Details

Jia, X., Wang, C., Zhao, C., Ge, Y. & Wallace, G. G. (2016). Toward biodegradable Mg-air bioelectric batteries composed of silk fibroin-polypyrrole film. Advanced Functional Materials, 26 (9), 1454-1462.

DOI: 10.1002/ (adfm.201503498)
Article type: Full Paper

Towards Biodegradable Mg-Air Bioelectric Batteries Composed of Silk Fibroin-Polypyrrole Film

Xiaoteng Jia, Caiyun Wang, Chen Zhao, Yu Ge, Gordon G. Wallace**

Xiaoteng Jia, Dr. Caiyun Wang, Chen Zhao, Yu Ge, Prof. Gordon G. Wallace
ARC Centre of Excellence for Electromaterials Science, Intelligent Polymer Research Institute, AIIM Facility, Innovation Campus, University of Wollongong, NSW 2522, Australia.
E-mail: caiyun@uow.edu.au (C.W.), gwallace@uow.edu.au (G.G.W.)

Keywords: silk fibroin, polypyrrole, biodegradable electrode, biodegradable battery, implantable medical device

Abstract:

Biodegradable active implantable devices can be used to diagnose and/or treat disease and eventually disappear without surgical removal. If an "external" energy source is required for effective operation then a biocompatible and biodegradable battery would be ideal. In this study, a partially biodegradable Mg-air bioelectric battery (bio-battery) was demonstrated using a silk fibroin-polypyrrole (SF-PPy) film cathode coupled with bioresorbable Mg alloy anode in phosphate buffered saline (PBS) electrolyte. Polypyrrole (PPy) is chemically coated onto one side of the silk substrate. SF-PPy film shows a conductivity of ~1.1 S cm^{-1} and a mild catalytic activity towards oxygen reduction. It degrades in a concentrated buffered

protease XIV solution, with a weight loss of 82% after 15 days. The assembled Mg-air bio-battery exhibit a discharge capacity up to 3.79 mA h cm^{-2} at a current of 10 μA cm^{-2} at room temperature, offering a specific energy density of ~4.70 mW h cm^{-2}. This novel partially biodegradable battery provides another step along the route to biodegradable batteries.

1. Introduction

Active implantable medical devices (AIMDs) provide therapy to treat, monitor or diagnose health conditions that challenging human life.[1] Most of them are chronic implants that are typically intended to stay in the human body for permanent use. The recent emergence of temporary implants, by contrast, features biodegradability in mild conditions at the end of their life.[2] When combined with electronically active components, these temporary implants may cater for various medical applications, such as wound healing, disease tracking, drug delivery and cardiovascular stimulators.[3] They should gradually disintegrate, dissolve, resorb or degrade after their use in a programmed fashion.[4] Biodegradability while preserving electrical functionality would avoid surgical removal and may reduce chronic inflammation[5].

To drive these biodegradable AIMDs, an implantable power source is indispensable. Batteries are currently used for chronic implants due to the high energy density available.[6] However, currently used structures contain toxic electrode materials. There is a need to develop biocompatible and biodegradable batteries. To date, very limited research progress has been achieved. Bettinger *et al.* reported an aqueous sodium-ion battery using the skin pigment melanin as the anode and manganese oxide as the cathode.[7] Such an edible battery breaks down into nontoxic components and generates potentials of 0.6 V for 5 h.[8] Rogers *et al.* developed a fully biodegradable primary battery with a dissolvable magnesium anode and

a molybdenum cathode.[9] The battery maintained a stable voltage up to 0.7 V for 24 h in PBS electrolyte. They all suffer from relatively short lifetime and low power density.

To power more sophisticated temporary implantable electronics, there is a need to develop biodegradable batteries with higher energy. A Mg-air bio-battery utilizing body fluid as electrolyte possesses a high theoretical voltage of 3.09 V and an energy density of 2840 W h kg^{-1}.[10] Mg is essential for biological function. It is biocompatible and has an acceptable dissolution rate in body fluid. Conducting polymers (CPs) serving as air cathodes in bio-batteries, possess the joint merits of biocompatibility[11] along an electrocatalytic activity towards oxygen reduction.[12] However, CPs are very stable under physiological condition, and cannot degrade via hydrolysis or enzymatic processes resulting from the action of cells.[13] A possible solution to this problem involves the fabrication of composites in which the biopolymer component provides controlled degradability, and wherein conductivity and electroactivity are provided by conducting polymer.

Silk fibroin (SF) is a sustainable biopolymer and a promising candidate for advanced implantable electronic devices interfaced within the body.[14] SF has been used as a biologically active substrate for the fabrication of bio-integrated electronics,[15] implantable cardiac electrophysiology[16] and transient silicon electronics.[17] Silk films are robust and have a programmable degradation lifetime that results in nontoxic amino acid products.[18] Silk films also have oxygen and water vapor permeability, [19] characteristics ideal as a CP substrate for bio-batteries. Biocompatible silk-PPy composites with a conductivity of 1 S cm^{-1} have recently been reported for use as electromechanical actuators.[20] A degradation profile of 8% mass loss after 10 days incubation in protease XIV solution (10 U mL^{-1}) was reported.[21]

Towards paving the way for a biocompatible and biodegradable battery, here we report a SF-PPy film as an air cathode material in a Mg-air bio-battery. In this SF-PPy film the PPy layer

was chemically coated onto one side of a silk film substrate. Upon enzymatic degradation an 82% weight loss is recorded after 15 days. The operation of the Mg-air bio-battery was evaluated.

2. Results and Discussion

2.1. Preparation and Characterization of SF-PPy Film

The silk film was prepared using a simple casting method from a 7.5 wt% SF solution. To render the silk film insoluble in water, a water-vapor annealing procedure was applied. This allows the fibroin chain to self-assemble into a structure with reduced *β*-sheet content, thus resulting in a rapid biodegradation rate.[22] SF-PPy film prepared by chemically coating a PPy layer only onto top side of silk support showed a bilayer structure with a total thickness of ~60 μm (**Figure 1**a). The glossy black PPy coating was composed of particles/aggregates (Figure 1b). The thickness of the PPy layer was about 7 μm (Figure 1c). The film substrate (referred to the back side of SF-PPy film) retained a smooth and uniform morphology after the polymerization; no obvious PPy product can be observed (Figure 1d). The SF-PPy film contained 3.9% (w/w) PPy. The sheet resistivity of SF-PPy film doped with sodium *p*-toluenesulfonate (*p*TS) was on the order of 1×10^3 Ω sq^{-1}. This value was on par with other biodegradable conductive composites with similar PPy content.[23] The SF-PPy film demonstrated a conductivity of ~1.1 S cm^{-1} measured by the four point probe method.

Fourier-transform infrared spectra equipped with attenuated total reflectance (ATR-FTIR) and Raman spectroscopy were used to further characterize SF-PPy film structure. The characteristic absorbance bands in FTIR spectra for silk secondary structures include 1650~1630 cm^{-1} for amide I (C=O stretching), 1540~1520 cm^{-1} for amide II (secondary N-H bending) and 1270~1230 cm^{-1} for amide III (C-N stretching).[24] The bare silk film and film

substrate exhibited similar absorption bands (**Figure 2**a). They both showed a strong peak at 1650 cm^{-1}, corresponding to the silk I structure. In the amide II region, one peak at 1540 cm^{-1} (silk I) appeared, with a shoulder at 1520 cm^{-1} (silk II). In the amide III region a peak at 1236 cm^{-1}, generally assigned to random coil-structures, was observed.[25] These results indicated that SF-PPy film was dominated by silk I structure (random coils and α-helices) over silk II (β-sheets). They were consistent with the previously reported water-annealed silk films.[22, 26] The PPy-modified side of SF-PPy film showed only PPy characteristic peaks due to its complete coverage on the silk substrate. It exhibited absorption peaks of C-N absorption at around 1293 cm^{-1}, PPy ring breathing at 1150 cm^{-1} and C-H in plane bending modes at about 1025 cm^{-1}. The band at 965 cm^{-1} was assigned to a fraction of PPy free from the influence of the dopant.[27]

Raman spectroscopy also provides a powerful tool to study surface composition. No significant differences were observed among the spectra collected for the bare silk film and film substrate (Figure 2b). They both showed a prominent peak at 2940 cm^{-1} ascribed to the C-H stretching. The amide I band appeared at 1665 cm^{-1}, and the amide III range showed a complex structure at 1277 and 1243 cm^{-1}.[28] This was a characteristic spectral pattern of SF with a prevailing silk I conformation, in good agreement with the IR results. After PPy deposition, the typical bands of PPy located at 1570 and 1324 cm^{-1}, assigned to C=C backbone stretching and ring-stretching were observed. The bands at 1046 and 927 cm^{-1} were attributed to C-H out-of-plane and in-plane deformation of PPy, respectively.[29]

The thermal behavior of silk film was affected by the PPy layer, as evidenced from the thermogravimetric analysis (TGA) results (**Figure 3**). PPy-*p*TS powder showed a high thermal stability. The weight loss was 5% at temperature up to 150 °C due to water evaporation. It was stable up to 290 °C, and 52% of the weight remained at 600 °C. The silk film underwent a nearly 10% weight loss at 150 °C, indicating a strong water-silk interaction

in silk I predominant structure. Then it underwent a rapid decomposition from 250 °C, and a 37% weight remaining at 600 °C. For SF-PPy film, the decomposition of polymer backbone moved to higher temperature compared to silk film, from 250 to 262 °C. Weight retention at 600 °C increased as well, from 37% to 42%. These results suggested that the PPy layer acted as a protective layer against thermal degradation.

2.2. Electrochemical and Electrocatalytic Properties of SF-PPy Film

The electrochemical property of SF-PPy film was evaluated using cyclic voltammetry (CV) in oxygen-saturated or nitrogen-saturated PBS electrolyte at a scan rate of 5 mV s^{-1} (**Figure 4**a). In N_2-saturated solution, a pair of redox peaks appeared at around -0.70 V and 0.30 V. These are related to the redox activity of PPy. In O_2-saturated solution, the cathodic peak increased in magnitude. The cathodic current increase can be ascribed to the enhanced redox properties of PPy in the presence of O_2. The reduced PPy (close to the fully dedoped state at -0.7 V) can be re-oxidized by oxygen (and oxygen is reduced concomitantly), and the conductivity of reduced PPy was enhanced resulting in an increased cathodic current density.[30]

To verify the electrocatalytic activity of SF-PPy film electrode, it was first reduced by applying constant potential of -0.85 V for 600 s. After removal of the applied potential, the open circuit potential (OCP) increased immediately. A higher potential increase could be observed in oxygen-rich solution. After 10 min of bubbling oxygen, the potential increased from -0.41 V to 0.03 V, compared to -0.14 V with no bubbling.

The Nyquist plots obtained using Electrochemical Impedance Spectroscopy (EIS) (Figure 4c) revealed a semicircular region lying on the real axis, which was followed by a straight line. An equivalent circuit model was used to analyze the impedance spectra (Figure 4d). In this

circuit, Rs was the bulk resistance; Rct was the charge transfer resistance. The constant phase elements CPE, was associated with double-layer capacitance across the film/electrolyte solution interfaces; Wo corresponded to the Warburg impedance resulting from the semi-infinite diffusion of ions at the electrode at low frequency.[31] Electrochemical parameters were simulated using Z-view software, and a good fit between the experimental results and the simulated equivalent circuit was shown (Figure 4c). The bulk resistance was about 82 Ω cm^{-2} and SF-PPy film showed a charge transfer resistance of 15 Ω cm^{-2}. Despite the insulating nature of silk substrate, the charge transfer resistance reported here was comparable to the PPy-*p*TS electrode (9.4 Ω cm^{-2}) on stainless steel (SS) mesh in PBS electrolyte, suggesting good conductivity and redox activity.[32]

2.3. Discharge Characteristics of Mg-Air Bio-Batteries Composed of SF-PPy Film

Galvanostatical discharge profiles of batteries at various current densities were investigated in PBS electrolyte at room temperature (**Figure 5**a). In this Mg-air battery system, PPy is the catalytic towards oxygen reduction. The factor determining battery performance is the corrosion rate of the Mg anode.[33] The capacity normalized in areal units is most appropriate to this work. The cell voltage was in the range of 1.79-1.72 V just after being assembled. This dropped immediately when a discharge current was applied and soon reached a flat discharge plateau. The voltages at the middle point of discharge curves ranged between 1.24 V and 1.10 V at the current range of 10-100 μA cm^{-2}. The assembled Mg-air bio-batteries exhibited a discharge capacity from 0.64 to 3.79 mA h cm^{-2}, offering a specific energy density up to ~4.70 mW h cm^{-2}. This bio-battery exhibited slightly lower middle point voltages and capacities (1.29-1.06 V, 4.42-0.93 mA h cm^{-2}) than the previously reported result with electrodeposited PPy-*p*TS cathode on SS mesh.[34] Nevertheless, it delivered a much higher stable voltage and specific capacity than those (0.4-0.7 V, 2.4 mA h cm^{-2}) from recently

reported biodegradable Mg-Mo battery.[9] We further investigated the rate capability (Figure 5b) at the range of 5 to 100 μA cm^{-2}. SF-PPy film delivered a relatively stable discharge plateaus at all these current densities, indicative of good stability as cathode material for bio-batteries. Plots of power density *vs.* current density were obtained (Figure 5c). The voltage used was obtained at the 4th hour during the 8 hours discharge. This bio-battery delivered a maximum power density of 64.6 μW cm^{-2} at a current density of 80 μA cm^{-2}. This power output was higher than that (39 μW cm^{-2}) reported for biodegradable electroplated Mg battery.[35] This battery could drive some types of commercial chronic AIMDs, such as cardiac pacemakers or bio-monitoring systems. Generally, the power requirements for these AIMDs fall in the level of micro- to milliwatts.[6]

2.4. Enzymatic Degradation of SF-PPy Film

To assess the biodegradation of SF-PPy film, we exposed it and silk films to a buffered protease XIV solution (1.0 mg mL^{-1}) (**Figure 6**a). After 24 h exposure, the weight loss of SF-PPy film was 24%; lower than the 42% for a pure silk film. In this stage, the weight loss can be attributed to the degradation of silk I and/or noncrystalline regions in SF.[36] The weights of both samples decreased slowly afterwards. The silk film was disintegrated after 5 days. SF-PPy film exhibited a much smaller weight loss, suggesting that PPy layer could slow down the degradation rate of SF. After 10 days, SF-PPy film lost 65% of its original weight, much higher than that (8%) previously reported for PPy coating on both side of silk substrate.[21] The role of degradation obtained can be attributed to the low β-sheet content in SF obtained via water annealing treatment and the unique bilayer structure of SF-PPy film, which facilitated the enzyme to attack the silk film with cleavage sites available on the surface. After 13 days incubation, SF-PPy film could not keep its original form and crumbled into small fractions due to the degradation of silk substrate. Figure 6b provides the images of

SF-PPy film or film debris on the filter paper after degradation in the protease XIV solution. The SF-PPy film kept its structural integrity and PPy layer was not delaminated from the silk substrate during 10 days incubation. Small irregular debris was present on the filter paper after 15 days degradation. All of the residual materials accounted for 18% of its starting weight. If SF-PPy film could be further degraded into several hundred nanometer pieces under optimized enzyme treatment, this material may eventually eliminated by renal excretion, phagocytosis and/or endocytosis.[37] We should mention that both the silk films and SF-PPy film incubated in PBS only were stable through the whole incubation period.

Structural changes after enzymatic degradation were investigated by ATR-FTIR. As demonstrated in Figure 6c, the dominant structure of film substrate was basically unchanged, but with some slight increase of β-sheet crystalline region probably due to the digestion of silk I and/or noncrystalline region in the silk substrate.[38] With the increased incubation time, the intensity of the amide I shoulder at 1630 cm^{-1} increased, indicating an enhancement in the degree of crystallinity.[39] After 10 days incubation, an interesting feature was observed that the film substrate showed a combined pattern of PPy and silk. This can be attributed to the degradation of silk substrate resulting in the exposure of PPy layer. The amide III (C-N stretching) band at 1236 cm^{-1} decreased gradually, which was considered markers for the amorphous structure of SF.[40] This band finally disappeared after 15 days incubation, whereas a new broad band for C-N stretching from PPy appeared at 1303 cm^{-1}.

To further understand the enzymatic degradation process, we observed surfaces morphologies by SEM. **Figure 7** showed representative images of SF-PPy film during the degradation as a function of time. Before incubation, both sides appeared to be even and uniform. After 5 days degradation, the film substrate experienced a rapid weight loss, resulting in cracks, whereas the PPy particles/aggregates on the SF-PPy film became smaller. After 15 days of continued surface corrosion, the residual sheets/debris was carefully collected by filtration and used for

examination. The film substrate showed the presence of larger surface stripping region and increased surface roughness associated with the extensive degradation (Figure 7c), confirming that the enzyme could penetrate and diffuse inside the swollen film matrix toward available cleavage sites. Several cavities were also observed on the SF-PPy film owing to the delamination of PPy particles from the substrate (Figure 7f). These results demonstrated that the overall enzymatic degradation of the silk component was mediated by surface erosion.[41]

To evaluate the effect of enzyme exposure, the electrical resistance was monitored during the incubation period in buffered protease XIV solution or PBS as controls (**Figure 8**a). The sheet resistivity increased from 0.6 to ~5.4 kΩ sq^{-1} upon 10 days exposure to the enzyme solution, roughly 9 times compared with its original value. The resistivity increase may be attributed to the disruption of continuous conductive PPy framework or the decreased affinity of PPy to silk substrate. Electrodes soaked in PBS electrolyte exhibited a much smaller increase (~0.8 kΩ sq^{-1}) during that period. These results demonstrated that SF-PPy film still retained electrical functionality throughout the 10 days of enzyme exposure. However, after 15 days incubation, the resistivity was hard to measure because of the physical disintegration of SF-PPy film.

To give a preliminary estimate of battery performance upon enzyme exposure, we conducted galvanostatically discharge tests in buffered protease XIV solution or PBS electrolyte at 37 °C (Figure 8b). The battery in the protease solution exhibited a discharge plateau (middle point of the discharge curve) of 1.14 V; lower than that (1.19 V) in PBS electrolyte at 37 °C. The protein molecular adsorbed on the electrodes surface can retard the electron/charge transfer process and thus slow down the redox reactions.[42] Therefore, a lower cell voltage and faster potential drop were observed. This battery maintained a steady output at 1.14 V at a current density of 20 μA cm^{-2} after exposed to the enzyme solution for 19.3 h. The power offered (22.8 μW cm^{-2}) may fulfill the requirements for average consumption of published

wireless implantable sensing systems (<0.5 V, <0.5 μW).[43] It was also noted that the battery in PBS electrolyte at 37 °C demonstrated a much lower capacity too, only ~21 % of that obtained at room temperature. It can be ascribed to the accelerated Mg dissolution rate and significant increase of hydrogen evolution induced at high temperature.

3. Conclusions

In this study, we demonstrate a novel air cathode material, PPy fabricated on a biodegradable silk film. The silk substrate supports the catalytic material (PPy) and provides a mean of controllable biodegradability. PPy was deposited only on one side of the silk substrate, thus providing the cleavage sites for the enzyme to attack. SF-PPy film undergoes degradation with an 82% weight loss after 15 days incubation in buffered protease XIV solution. Degradation of the silk substrate leads to fracture and disintegration of the SF-PPy film, thereby offering the possibility to be eliminated by renal excretion, phagocytosis and/or endocytosis without surgical removal. This approach can be used to fabricate other types of electrodes based on biocompatible conducting polymers with good catalytic activity towards oxygen reduction, such as poly(3,4-ethylenedioxythiophene). These results highlight the feasibility of realizing a biodegradable battery when coupled with bioresorbable Mg alloy, which could provide appropriate power coupled with the required degradation profile. Developments in the area of biodegradable battery structures together with implantable medical devices will open up new possibilities for biomedical research and clinical care.

4. Experimental Section

Materials: Bombyx mori silkworm cocoons were purchased from Peaceful Silkworms, Australia. Protease type XIV from *Streptomyces griseus*, PBS tablet and pyrrole were

purchased from Sigma-Aldrich. Pyrrole was freshly distilled. The PBS electrolyte (pH 7.4 at 25 °C) was prepared by dissolving one PBS tablet in Milli-Q water (18.2 MΩ·cm) (200 mL). Magnesium alloy (AZ31) sheet with the nominal mass composition 96% Mg, 3% Al and 1% Zn was purchased from Goodfellow Metals, UK. It was polished with fine sandpaper and degreased with acetone prior to use.

Preparation of Water-stable Silk Film: Regenerated SF aqueous solution (concentration *ca.* 7.5 wt%) was prepared from *B. mori* silkworm cocoons according to the procedures described in the literature.[44] To prepare solid silk films, aqueous silk solution (2.5 mL) was cast onto a Teflon mold and dried at room temperature for 24 h. These dried films were subjected to a water-vapor annealing process for 24 h to induce the formation of silk I and silk II structures. The film thickness is in the range of 45-55 μm.

Chemical Deposition of PPy on Silk Film with a Bilayer Structure: A PPy layer was chemically deposited on silk film. To achieve a bilayer structure, the bottom side of silk film was sealed with polyimide film (Kapton tape, Ted Pella) and then adhered onto the container wall to avoid reaction solution reaching the back side. Films were exposed to an aqueous solution (45 mL) containing pyrrole and *p*TS. Ethanol (5 mL) was added to improve the wettability of silk film. The solution was kept stirring in an ice bath for 30 min, followed by adding a pre-cooled $FeCl_3$ solution (5 mL) drop-wise to initiate the polymerization. The reaction was performed in an ice-bath for 4 h. The concentration of pyrrole, $FeCl_3$ or *p*TS was 0.1 M. The obtained film was washed with abundant deionized (DI) water, followed by sonication in DI water for 30 min to remove any loosely bounded PPy. Finally, the film was dried at room temperature overnight. PPy-*p*TS powder was synthesized using the same conditions as above. After 4 h polymerization, black precipitate was formed. PPy-*p*TS powder was collected by filtration and rinsed with DI water several times. It was dried overnight at room temperature.

Characterization and Properties of SF-PPy Film: The surface and cross-section morphologies of the SF-PPy film were investigated using FE-SEM (JEOL JSM-7500FA). Samples were dehydrated under vacuum at 50 °C for 24 h. Films were sputter coated with Au for 40 s using an Edwards Auto 306 Sputter Coater. The tilted cross-sectional view (approximately 20^{o}) of SF-PPy film was characterized using an optical microscope (Leica DM6000). FTIR measurements were recorded with a Shimadzu AIM8000 spectrometer equipped with an ATR accessory. Raman spectroscopy was performed using a JOBIN YVON HR800 Confocal Raman system with 632.8 nm diode laser excitation on a 300 lines/mm grating at room temperature. TGA was conducted by heating the samples from 30 to 600 °C at a heating rate of 5 °C min^{-1} under N_2 using a Q500 TGA analyser (TA Instruments, UK).

Sheet resistivity (R, Ω sq^{-1}) of SF-PPy film was measured with a Jandel RM3 Conductivity Meter using a four-point probe method. The thickness (d, cm) of PPy coating was obtained from SEM and used to calculate the conductivity (σ, S cm^{-1}) of SF-PPy film, using the equation $\sigma = 1 / (R \cdot d)$. CV of SF-PPy film was conducted using an electrochemical workstation (CHI 650D). EIS for SF-PPy film was measured using a Gamry EIS 3000 system in the frequency range of 25 kHz to 0.01 Hz with an AC perturbation of 5 mV. They were all performed in a conventional three-electrode cell with a SS mesh counter electrode and a Ag/AgCl (3 M NaCl) reference electrode. The effect of oxygen on the reduced SF-PPy film was investigated by monitoring the open-circuit potential in oxygen saturated, air saturated or normal PBS electrolytes (no gas disturbance), similar to the work reported by Wu *et al*.[45] SF-PPy film was firstly reduced at -0.85 V (*vs.* Ag/AgCl) for 600 s, followed by gas introduction if applied. The gas flow rate was controlled at 200 mL min^{-1}.

Cell Construction and Testing: The cell was fabricated with a Mg alloy anode (10 mm × 10 mm) and SF-PPy film cathode (10 mm × 10 mm) in a one compartment cell with PBS

electrolyte (20 mL), and tested using a battery-testing device (Neware Electronic Co.). It was discharged galvanostatically to a cut-off cell voltage of 1.0 V at room temperature. For rate capability testing, the cell was discharged for 8 hour at various current densities without a cut-off voltage applied. An idle time of 0.5 hour (no applied current) was used between each step. The cell discharge performance was also investigated at 37 °C in 1.0 mg mL^{-1} protease XIV PBS solution (20 mL) or PBS only electrolyte as controls. The applied current was 20 μA cm^{-2} and the cut-off cell voltage was 1.0 V.

Enzymatic Degradation of SF-PPy Film: SF-PPy films and silk films (N=3 per group and time point) were dried under vacuum at 50 °C for 24 h, and then immersed in buffered protease XIV solutions (5 mL). The protease XIV was dissolved in PBS solution to prepare the enzyme solution (1.0 mg mL^{-1}). Samples (10 mm × 10 mm × 0.06 mm, mass of 10 ± 2 mg) were incubated in this solution at 37 °C. Enzyme solutions were refreshed daily for 15 days. At designated times; samples were taken out, washed with DI water, dried under vacuum at 50 °C for 24 h and weighed. The degradation rate was calculated as the ratio of weight after digestion to the original weight of the samples. Samples in PBS solution were used as controls following the same procedures. The chemical structure of the substrate after biodegradation was determined by ATR-FTIR. Morphological changes were observed using SEM. The electrical resistance of SF-PPy film was measured using a four-point probe method.

Acknowledgements

Funding from the Australian Research Council Centre of Excellence Scheme (Project Number CE 140100012) is gratefully acknowledged. G.G.W. is grateful to the ARC for support under the Australian Laureate Fellowship scheme (FL110100196). The authors

would like to thank the Australian National Nanofabrication Facility-Materials node (ANFF) and the UoW Electron Microscopy Centre for equipment use.

References

[1] M. R. Sohail, D. Z. Uslan, A. H. Khan, P. A. Friedman, D. L. Hayes, W. R. Wilson, J. M. Steckelberg, S. Stoner, L. M. Baddour, *J. Am. Coll. Cardiol.* **2007**, *49*, 1851-1859.

[2] a) A. Lendlein, R. Langer, *Science* **2002**, *296*, 1673-1676; b) M. Moravej, D. Mantovani, *Int. J. Mol. Sci.* **2011**, *12*, 4250-4270.

[3] a) H. Tao, S. W. Hwang, B. Marelli, B. An, J. E. Moreau, M. M. Yang, M. A. Brenckle, S. Kim, D. L. Kaplan, J. A. Rogers, F. G. Omenetto, *Proc. Natl. Acad. Sci. U. S. A.* **2014**, *111*, 17385-17389; b) L. Z. Xu, S. R. Gutbrod, A. P. Bonifas, Y. W. Su, M. S. Sulkin, N. S. Lu, H. J. Chung, K. I. Jang, Z. J. Liu, M. Ying, C. Lu, R. C. Webb, J. S. Kim, J. I. Laughner, H. Y. Cheng, Y. H. Liu, A. Ameen, J. W. Jeong, G. T. Kim, Y. G. Huang, I. R. Efimov, J. A. Rogers, *Nat. Commun.* **2014**, *5*, 3329.

[4] a) C. J. Bettinger, Z. A. Bao, *Adv. Mater.* **2010**, *22*, 651-655; b) M. Irimia-Vladu, *Chem. Soc. Rev.* **2014**, *43*, 588-610; c) S. W. Hwang, G. Park, H. Cheng, J. K. Song, S. K. Kang, L. Yin, J. H. Kim, F. G. Omenetto, Y. G. Huang, K. M. Lee, J. A. Rogers, *Adv. Mater.* **2014**, *26*, 1992-2000.

[5] a) C. R. Gordijo, A. J. Shuhendler, X. Y. Wu, *Adv. Funct. Mater.* **2010**, *20*, 1404-1412; b) A. Sokolov, B. C. Hellerud, E. A. Johannessen, T. E. Mollnes, *J. Biomed. Mater. Res., Part A* **2012**, *100A*, 1142-1150.

[6] X. Wei, J. Liu, *Front. Energy Power Eng. China* **2008**, *2*, 1-13.

[7] Y. J. Kim, W. Wu, S. E. Chun, J. F. Whitacre, C. J. Bettinger, *Proc. Natl. Acad. Sci. U. S. A.* **2013**, *110*, 20912-20917.

[8] Y. J. Kim, S. E. Chun, J. Whitacre, C. J. Bettinger, *J. Mater. Chem. B* **2013**, *1*, 3781-

3788.

[9] L. Yin, X. Huang, H. X. Xu, Y. F. Zhang, J. Lam, J. J. Cheng, J. A. Rogers, *Adv. Mater.* **2014**, *26*, 3879-3884.

[10] a) C. Y. Wang, W. Zheng, Z. L. Yue, C. O. Too, G. G. Wallace, *Adv. Mater.* **2011**, *23* 3580-3584; b) Y. Kong, C. Y. Wang, Y. Yang, C. O. Too, G. G. Wallace, *Synth. Met.* **2012**, *162*, 584-589.

[11] a) W. W. Hu, Y. T. Hsu, Y. C. Cheng, C. Li, R. C. Ruaan, C. C. Chien, C. A. Chung, C. W. Tsao, *Mater. Sci. Eng., C* **2014**, *37*, 28-36; b) A. Vaitkuviene, V. Kaseta, J. Voronovic, G. Ramanauskaite, G. Biziuleviciene, A. Ramanaviciene, A. Ramanavicius, *J. Hazard. Mater.* **2013**, *250*, 167-174.

[12] Y. F. Li, R. Y. Qian, *Synth. Met.* **1989**, *28*, C127-C132.

[13] R. Balint, N. J. Cassidy, S. H. Cartmell, *Acta Biomater.* **2014**, *10*, 2341-2353.

[14] H. Tao, D. L. Kaplan, F. G. Omenetto, *Adv. Mater.* **2012**, *24*, 2824-2837.

[15] D. H. Kim, J. Viventi, J. J. Amsden, J. L. Xiao, L. Vigeland, Y. S. Kim, J. A. Blanco, B. Panilaitis, E. S. Frechette, D. Contreras, D. L. Kaplan, F. G. Omenetto, Y. G. Huang, K. C. Hwang, M. R. Zakin, B. Litt, J. A. Rogers, *Nat. Mater.* **2010**, *9*, 511-517.

[16] D. H. Kim, R. Ghaffari, N. S. Lu, S. D. Wang, S. P. Lee, H. Keum, R. D'Angelo, L. Klinker, Y. W. Su, C. F. Lu, Y. S. Kim, A. Ameen, Y. H. Li, Y. H. Zhang, B. de Graff, Y. Y. Hsu, Z. J. Liu, J. Ruskin, L. Z. Xu, C. Lu, F. G. Omenetto, Y. G. Huang, M. Mansour, M. J. Slepian, J. A. Rogers, *Proc. Natl. Acad. Sci. U. S. A.* **2012**, *109*, 19910-19915.

[17] S. W. Hwang, H. Tao, D. H. Kim, H. Y. Cheng, J. K. Song, E. Rill, M. A. Brenckle, B. Panilaitis, S. M. Won, Y. S. Kim, Y. M. Song, K. J. Yu, A. Ameen, R. Li, Y. W. Su, M. M. Yang, D. L. Kaplan, M. R. Zakin, M. J. Slepian, Y. G. Huang, F. G.

Omenetto, J. A. Rogers, *Science* **2012**, *337*, 1640-1644.

[18] a) C. Vepari, D. L. Kaplan, *Prog. Polym. Sci.* **2007**, *32*, 991-1007; b) G. H. Altman, F. Diaz, C. Jakuba, T. Calabro, R. L. Horan, J. S. Chen, H. Lu, J. Richmond, D. L. Kaplan, *Biomaterials* **2003**, *24*, 401-416.

[19] N. Minoura, M. Tsukada, M. Nagura, *Biomaterials* **1990**, *11*, 430-434.

[20] I. S. Romero, N. P. Bradshaw, J. D. Larson, S. Y. Severt, S. J. Roberts, M. L. Schiller, J. M. Leger, A. R. Murphy, *Adv. Funct. Mater.* **2014**, *24*, 3866-3873.

[21] I. S. Romero, M. L. Schurr, J. V. Lally, M. Z. Kotlik, A. R. Murphy, *Acs Appl. Mater. Interfaces* **2013**, *5*, 553-564.

[22] X. Hu, K. Shmelev, L. Sun, E. S. Gil, S. H. Park, P. Cebe, D. L. Kaplan, *Biomacromolecules* **2011**, *12*, 1686-1696.

[23] a) G. X. Shi, M. Rouabhia, Z. X. Wang, L. H. Dao, Z. Zhang, *Biomaterials* **2004**, *25*, 2477-2488; b) B. L. Guo, L. Glavas, A. C. Albertsson, *Prog. Polym. Sci.* **2013**, *38*, 1263-1286.

[24] S. W. Ha, A. E. Tonelli, S. M. Hudson, *Biomacromolecules* **2005**, *6*, 1722-1731.

[25] D. Wilson, R. Valluzzi, D. Kaplan, *Biophys. J.* **2000**, *78*, 2690-2701.

[26] H. J. Jin, J. Park, V. Karageorgiou, U. J. Kim, R. Valluzzi, D. L. Kaplan, *Adv. Funct. Mater.* **2005**, *15*, 1241-1247.

[27] R. G. Davidson, T. G. Turner, *Synth. Met.* **1995**, *72*, 121-128.

[28] P. Monti, G. Freddi, A. Bertoluzza, N. Kasai, M. Tsukada, *J. Raman Spectrosc.* **1998**, *29*, 297-304.

[29] Y. C. Liu, B. J. Hwang, *Synth. Met.* **2000**, *113*, 203-207.

[30] V. G. Khomenko, V. Z. Barsukov, A. S. Katashinskii, *Electrochim. Acta* **2005**, *50*, 1675-1683.

[31] J. R. Macdonald, *Solid State Ionics* **2005**, *176*, 1961-1969.

[32] Y. Yang, C. Y. Wang, B. B. Yue, S. Gambhir, C. O. Too, G. G. Wallace, *Adv. Energy Mater.* **2012**, *2*, 266-272.

[33] T. R. Zhang, Z. L. Tao, J. Chen, *Mater. Horiz.* **2014**, *1*, 196-206.

[34] X. T. Jia, Y. Yang, C. Y. Wang, C. Zhao, R. Vijayaraghavan, D. R. MacFarlane, M. Forsyth, G. G. Wallace, *Acs Appl. Mater. Interfaces* **2014**, *6*, 21110-21117.

[35] M. Tsang, A. Armutlulu, F. Herrault, R. H. Shafer, S. A. B. Allen, M. G. Allen, *J. Microelectromech. Syst.* **2014**, *23*, 1281-1289.

[36] Q. Lu, X. Hu, X. Q. Wang, J. A. Kluge, S. Z. Lu, P. Cebe, D. L. Kaplan, *Acta Biomater.* **2010**, *6*, 1380-1387.

[37] a) S. Kim, W. K. Oh, Y. S. Jeong, J. Y. Hong, B. R. Cho, J. S. Hahn, J. Jang, *Biomaterials* **2011**, *32*, 2342-2350; b) Y. S. Jeong, W. K. Oh, S. Kim, J. Jang, *Biomaterials* **2011**, *32*, 7217-7225, c) H. T. Nguyen, S. Sapp, C. Wei, J. K. Chow, A. Nguyen, J. Coursen, S. Luebben, E. Chang, R. Ross, C. E. Schmidt, *J. Biomed. Mater. Res. A* **2014**, *102*, 2554-2564.

[38] M. Z. Li, M. Ogiso, N. Minoura, *Biomaterials* **2003**, *24*, 357-365.

[39] Q. A. Lu, B. Zhang, M. Z. Li, B. Q. Zuo, D. L. Kapan, Y. L. Huang, H. S. Zhu, *Biomacromolecules* **2011**, *12*, 1080-1086.

[40] T. Arai, G. Freddi, R. Innocenti, M. Tsukada, *J. Appl. Polym. Sci.* **2004**, *91*, 2383-2390.

[41] Y. Cao, B. C. Wang, *Int. J. Mol. Sci.* **2009**, *10*, 1514-1524.

[42] D. L. Miller, J. O. Bockris, *J. Electrochem. Soc.* **1992**, *139*, 967-976.

[43] Y. Lee, S. Bang, I. Lee, Y. Kim, G. Kim, M. H. Ghaed, P. Pannuto, P. Dutta, D. Sylvester, D. Blaauw, *IEEE J. Solid-State Circuits* **2013**, *48*, 229-243.

[44] D. N. Rockwood, R. C. Preda, T. Yucel, X. Q. Wang, M. L. Lovett, D. L. Kaplan, *Nat. Protoc.* **2011**, *6*, 1612-1631.

[45] A. Wu, E. C. Venancio, A. G. MacDiarmid, *Synth. Met.* **2007**, *157*, 303-310.

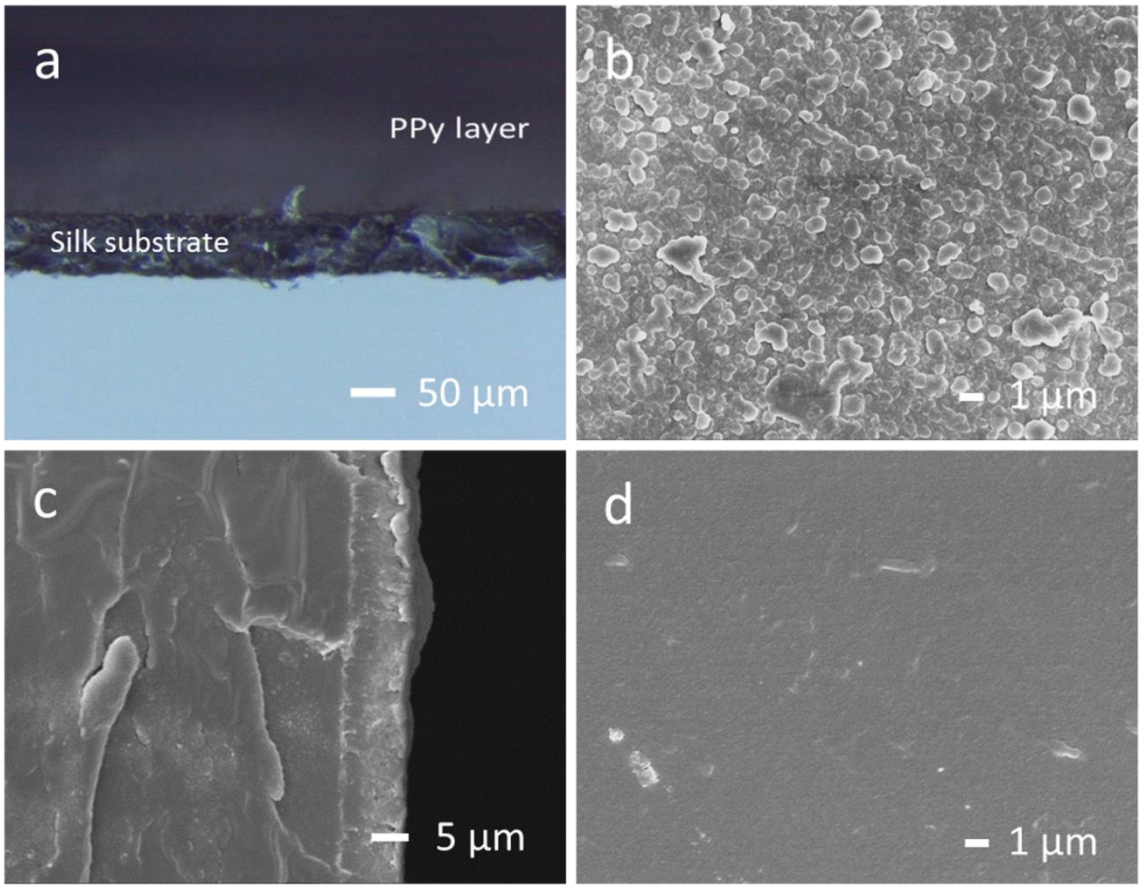

Figure 1 (a) Optical image of cross sectional view (20^{o} tilted) of SF-PPy film, scanning electron microscope images (SEM) of (b) PPy-modified side, (c) cross section and (d) back side of SF-PPy film.

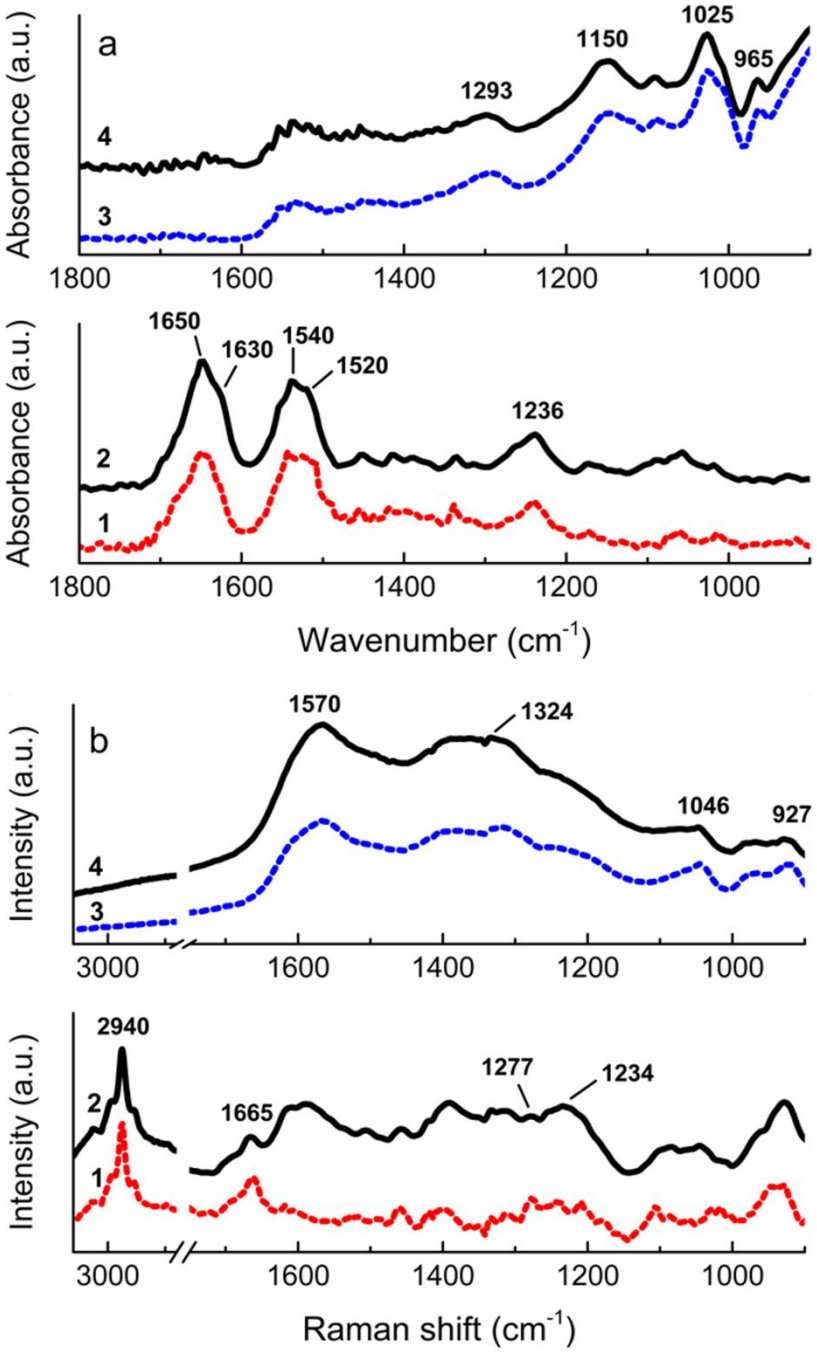

Figure 2 ATR-FTIR spectra (a) and Raman spectra (b) of bare water-annealed silk film (1), the film substrate (2), PPy-*p*TS powder (3) and PPy-modified side of SF-PPy film (4).

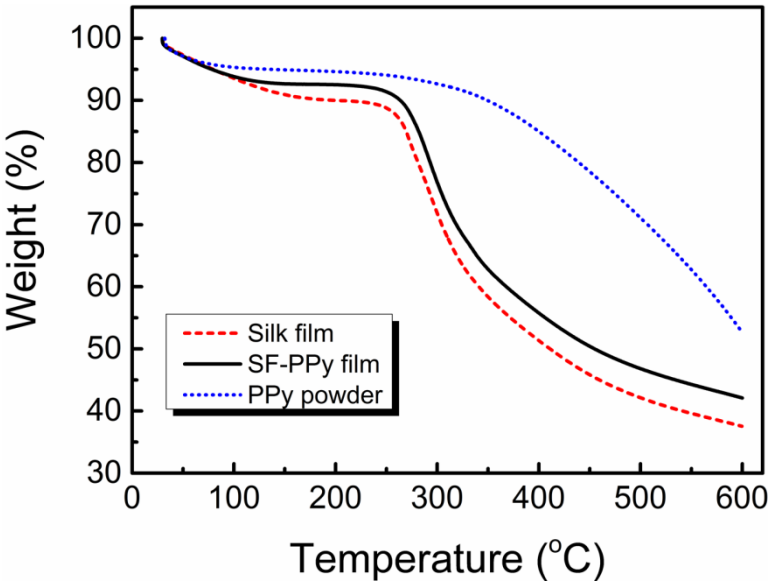

Figure 3 TGA curves of silk film, SF-PPy film and PPy-*p*TS powder.

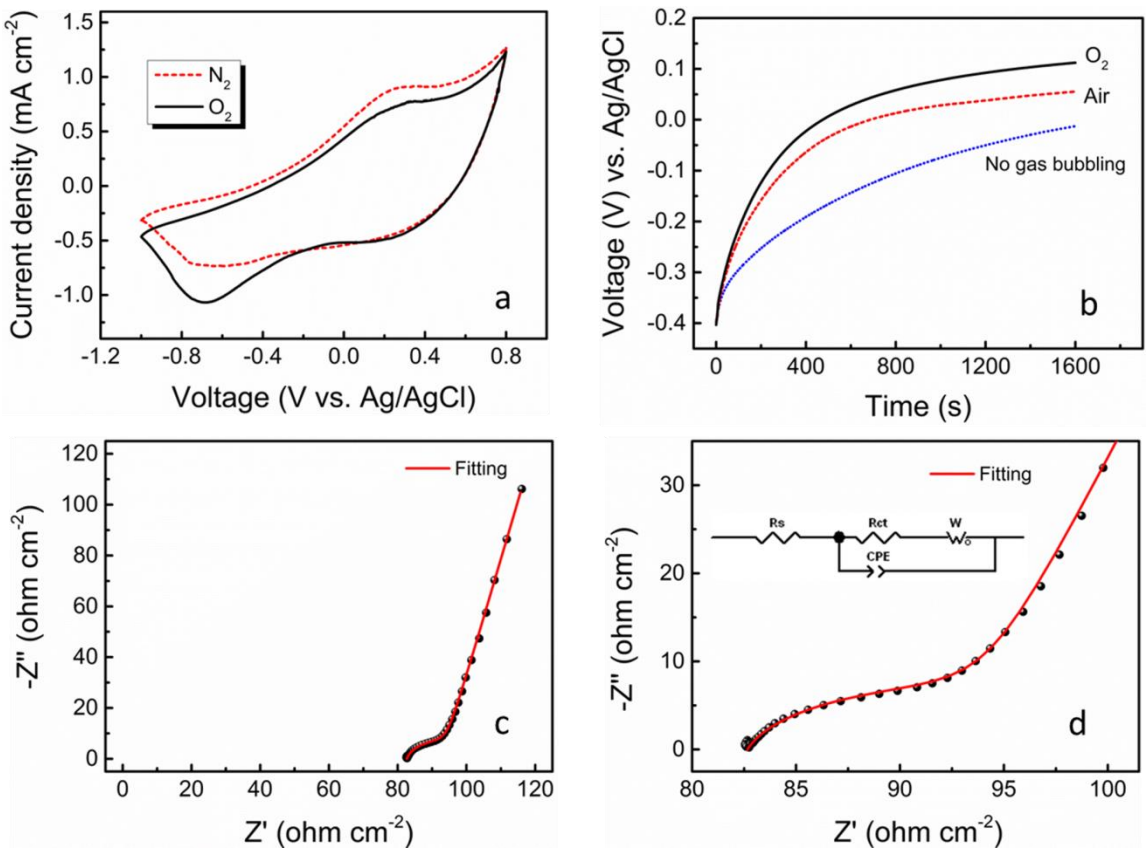

Figure 4 (a) CV of SF-PPy film in N_2- or O_2-saturated PBS electrolyte at a scan rate of 5 mV s^{-1}. (b) Potential response of reduced SF-PPy film in PBS electrolyte with N_2, O_2 or no gas bubbling after the applied potential (-0.85 V *vs.* Ag/AgCl) was removed. (c) EIS spectra and the simulated spectra (lines) of SF-PPy film in PBS electrolyte. (d) Expanded view EIS spectra and the simulated spectra (lines) at high frequency region, inset shows the equivalent circuit used for the simulation.

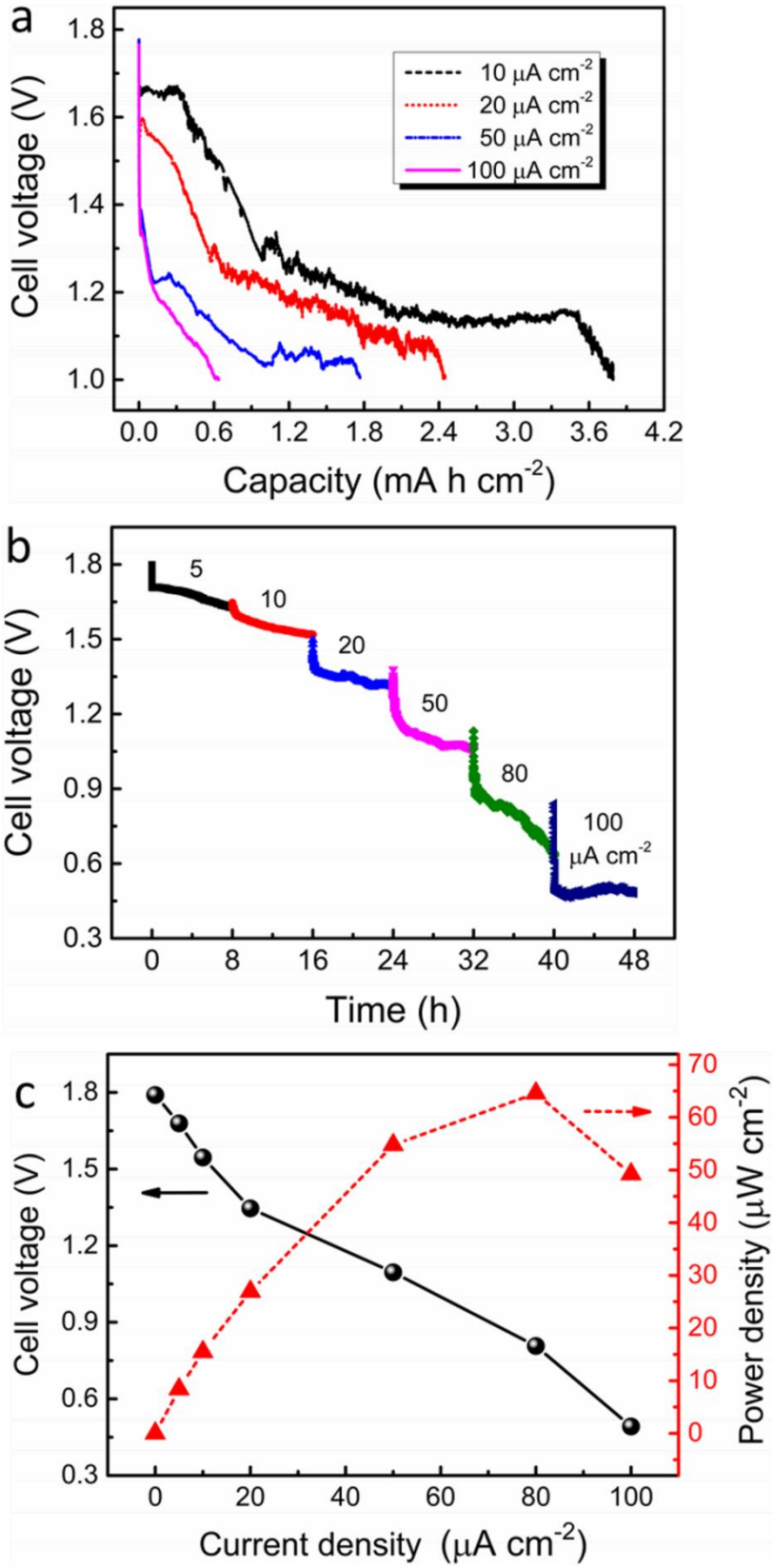

Figure 5 Galvanostatically discharge curves (a), rate capabilities (b), plateau voltage and the corresponding power density (c) of Mg-air bio-batteries composed of SF-PPy film at various current densities in PBS electrolyte at room temperature.

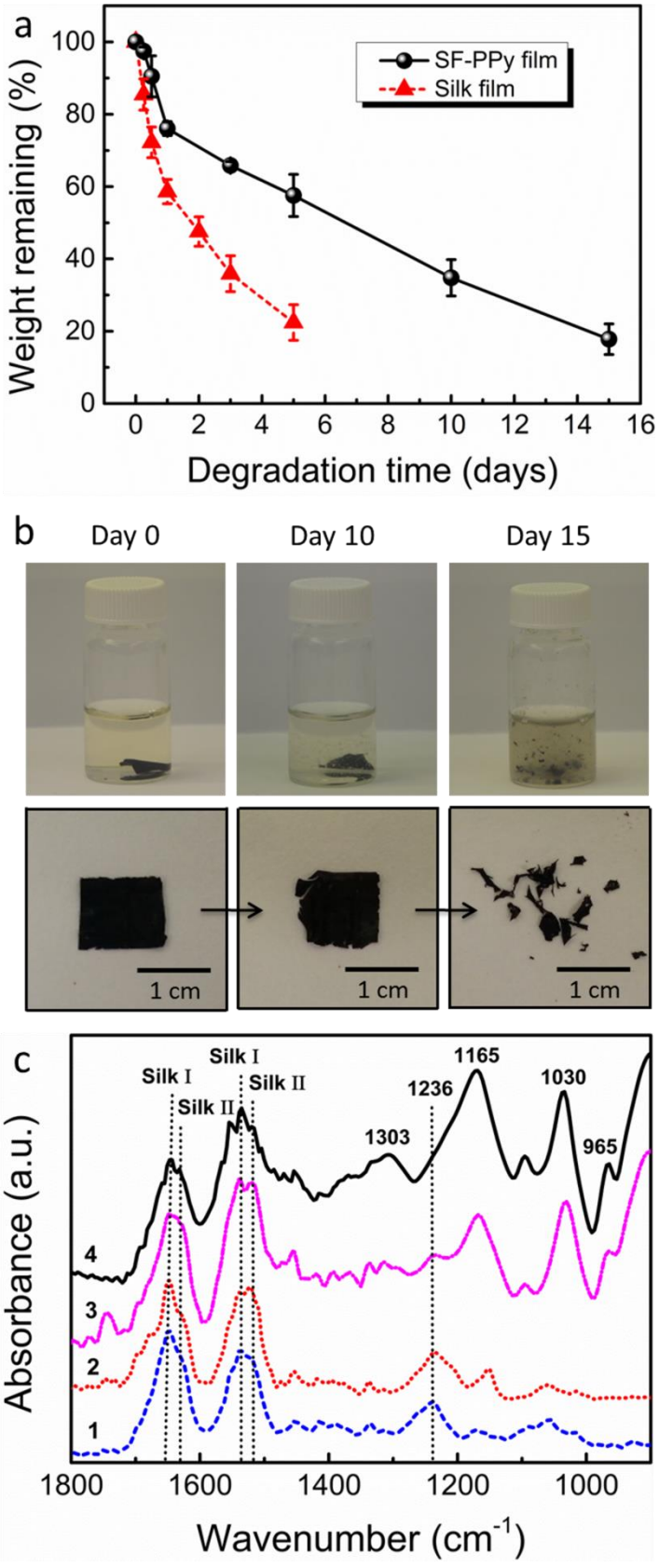

Figure 6 (a) Quantitative changes of silk film and SF-PPy film cultivated in buffered 1.0 mg mL^{-1} protease XIV solution, n=3, bars represent standard deviation; (b) Optical images of SF-

PPy film in the protease XIV solution (upper) and recovered on filter paper (lower) upon biodegradation; (c) ATR-FTIR spectra of the pristine film substrate (1), after incubation in the protease XIV solution for 5 days (2), 10 days (3) and 15 days (4) in the protease XIV solution.

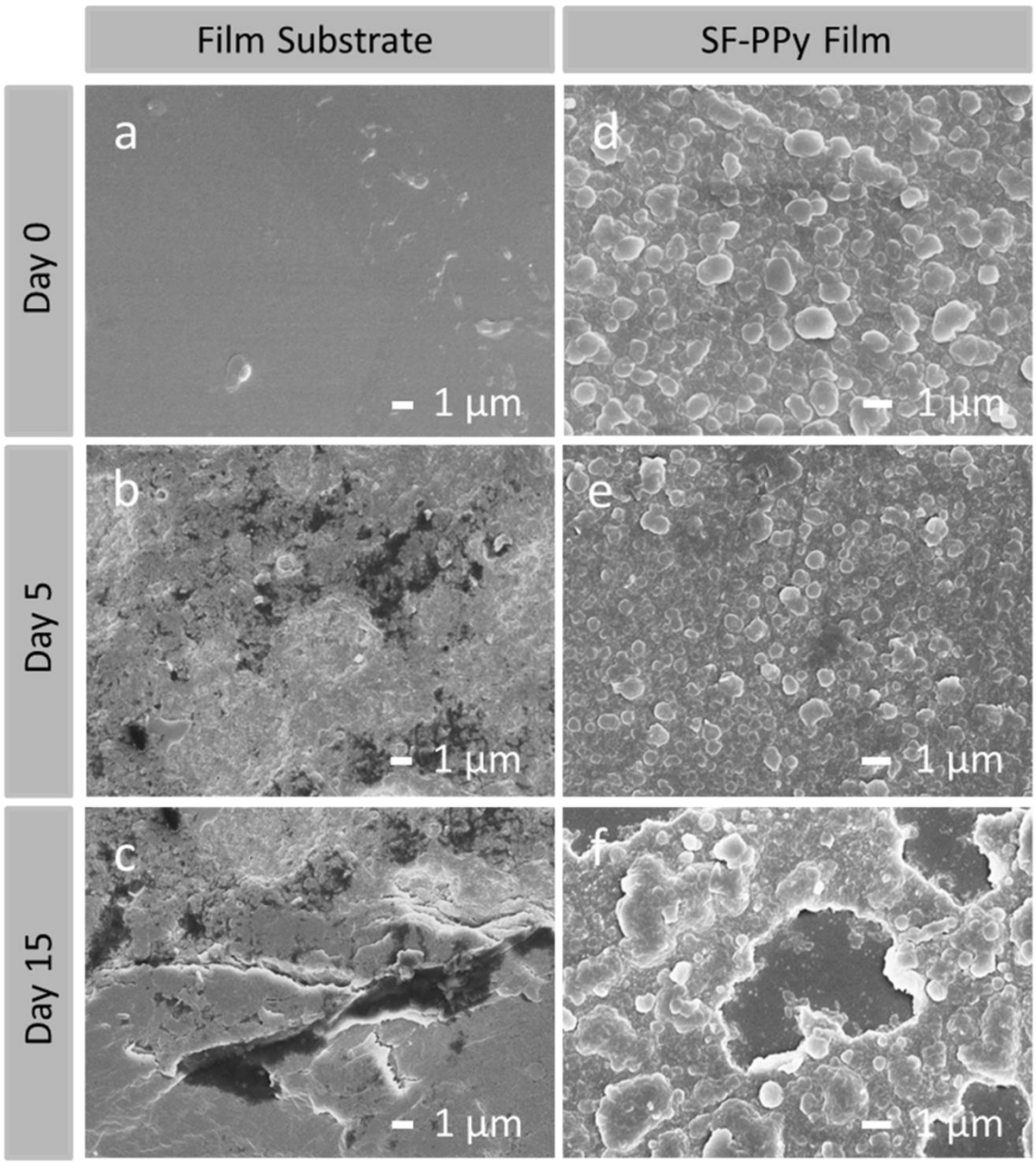

Figure 7 SEM images of the film substrate (a-c) and SF-PPy film (d-f) after cultivated in buffered protease XIV solution at various stages of degradation.

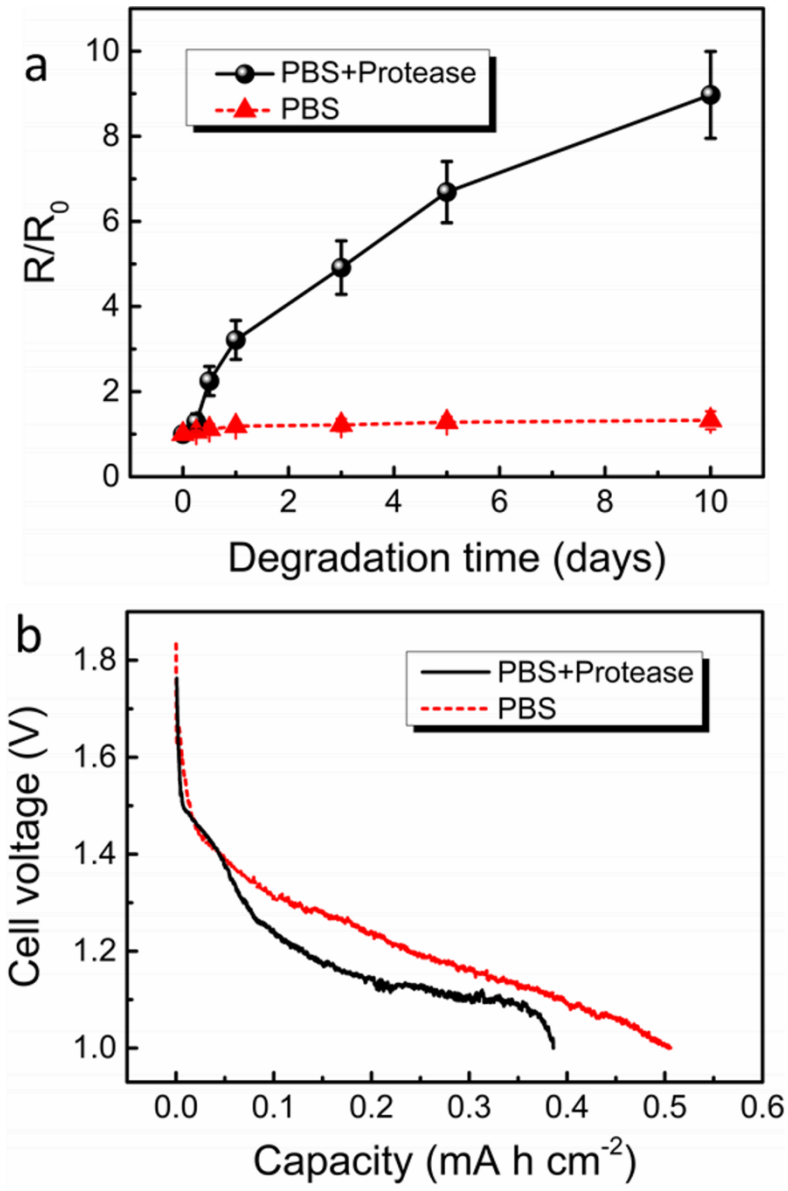

Figure 8 (a) Electrical resistance (R) of SF-PPy film incubated in buffered 1.0 mg mL^{-1} protease XIV solution or PBS over 10 days with respect to their original values (R_0), n=3, bars represent standard deviation; (b) Discharge performance of Mg-air bio-batteries composed of SF-PPy film at a current density of 20 μA cm^{-2} in buffered 1.0 mg mL^{-1} protease XIV solution or PBS electrolyte at 37 °C.

TOC

A partially biodegradable bilayer-structured film composed of silk fibroin and polypyrrole demonstrates a 82% mass loss after 15 days incubation in buffered protease XIV solution. It can offer an energy density of ~4.70 mW h cm^{-2} when coupled with Mg alloy in PBS. This battery system may provide appropriate power for temporary implantable electronics coupled with the required degradation profile.

Keyword: Batteries; Biomedical Applications; Conducting Polymers; Electrodes

Xiaoteng Jia, Caiyun Wang*, Chen Zhao, Yu Ge, Gordon G. Wallace*

Towards Biodegradable Mg-Air Bioelectric Batteries Composed of Silk Fibroin-Polypyrrole Film

ToC figure